Noncontact Physiological Dynamics Detection Using Low-power Digital-IF Doppler Radar

Heng Zhao, *Student Member, IEEE*, Hong Hong, *Member, IEEE*, Li Sun, *Member, IEEE*, Yusheng Li, *Member, IEEE*, Changzhi Li, *Senior Member, IEEE*, and Xiaohua Zhu, *Member, IEEE*

***Abstract*— The instantaneous vital sign rates, which are related to physiological dynamics, are important indicators of human health condition. This paper presents a noncontact way to measure the human instantaneous vital signs using digital-intermediate frequency (IF) Doppler radar. The synchrosqueezing transform-based algorithm has been proposed to get a concentrated time–frequency (TF) distribution, so that the high-resolution instantaneous heartbeat and respiratory rates and the time-domain signals can be acquired. Moreover, the developed radar with customized radio frequency module employs the direct IF sampling technique to achieve high sensitivity to capture the tiny vital sign variations. Experiments with different human subjects and physiological conditions have been carried out. Compared with the landmark-based method and traditional TF algorithms, the results show that instantaneous vital signs can be acquired more accurately within 3 m at a −13 dBm transmit power by the proposed method. Therefore, the radar can be used for evaluating the physiological dynamics and assessing health condition.**

***Index Terms*— Doppler radar, instantaneous vital sign, noncontact vital sign detection, synchrosqueezing transform (SST), time–frequency (TF) analysis.**

I. Introduction

BIOMEDICAL signals, especially respiratory and heartbeat signals, imply a lot of physiological information. These kinds of signals, which have oscillatory features, have been proved to be valuable for diagnosis and prognosis of some diseases [1]. Among various features hidden in the biomedical signals, the instantaneous breath rate (BR) and heartbeat rate (HR), along with their variabilities, are related to the physiological dynamics [2], [3]. These parameters can be indicators of human health condition.

The traditional method to acquire vital sign signals is using contact sensors, for example, electrocardiograph (ECG) and breath belt [4], [5]. Even though the results are moderately accurate, these sensors may cause discomfort and skin irritation to subject, which limit their applications to some special patients suffering from empyrosis and burn. Recently, the noncontact vital sign detection technology has attracted growing interests in various applications such as sleep monitoring, elderly care, earthquake rescue, border patrol, and entrance security [6]. Fundamentally, this technology utilizes the Doppler radar to emit an electromagnetic signal to human body. Then it captures the reflected signal and retrieves the involved physiological signals [7].

Most efforts in this field can be divided into two categories: system architecture design and signal processing algorithm development. Compared with the ultrawideband radar [8], [9], homodyne continuous-wave (CW) Doppler radar is widely used due to its simple structure. In [10] and [11], a single-chip silicon Doppler radar and a Ka-band heartbeat sensor were proposed, which validated the feasibility and analyzed the potential problems. Afterward, based on these work, various techniques have been applied to improve the radar performance [12]–[15]. Recently, the CW radar was used for motion-adaptive cancer radiotherapy [16], which broadened the application of CW Doppler radar.

However, these homodyne radar sensors encounter some problems such as quadrature channel imbalance and dc offset [17], which decrease the demodulation linearity. Fortunately, the digital radar receiver with direct intermediate-frequency (IF)-to-digital conversion (IF sampling) is a proper alternate [18]. The receiver first downconverts the radio frequency (RF) signal to an IF frequency, and then it samples the analog IF signal directly and accomplishes the subsequent signal processing in the digital domain. Owing to the reduction in the number of analog circuits, the accuracy and stability can be greatly improved. An instrument-based digital-IF Doppler radar was proposed in [19]. However, it is inaccurate due to the mismatch between different instruments.

Compared with the various system architectures, the baseband signal processing algorithm attracts little attention. Most of them are based on the discrete Fourier transform (DFT) [6]. Due to the smearing and leakage problems caused by limited data length, the DFT will suffer significant performance degradation in accuracy and resolution. Afterward, the RELAX algorithm was applied to improve the resolution [20]. But it did not tackle the time-varying vital sign rates. In [21] and [22], the compressed sensing (CS) theory is applied to extract the vital sign frequencies, which reduces the time window into 5 s.

Manuscript received June 12, 2016; revised September 25, 2016; accepted December 29, 2016. This work was supported in part by the National Science Foundation under Grant ECCS-1254838, in part by the Special Foundation of China Post-Doctoral Science under Grant 2013T6054, in part by the National Natural Science Foundation of China under Grant 61301022, in part by the National Key Technology Support Program under Grant 2015BAI02B04, and in part by the Natural Science Foundation of Jiangsu Province under Grant BK20140801. The Associate Editor coordinating the review process was Dr. Sasan Bakhtiari.

H. Zhao, H. Hong, L. Sun, Y. Li, and X. Zhu are with the School of Electronic and Optical Engineering, Nanjing University of Science and Technology, Nanjing 210094, China (e-mail: hongnju@njust.edu.cn).

C. Li is with the Department of Electrical Engineering, Texas Tech University, Lubbock, TX 79409 USA (e-mail: changzhi.li@ttu.edu).

Color versions of one or more of the figures in this paper are available online at http://ieeexplore.ieee.org.

Digital Object Identifier 10.1109/TIM.2017.2669699

But it still assumes the invariability of vital signs over a short duration. Consequently, it may be possible to blur the information if vital signs vary remarkably within the short duration.

In practice, the respiratory and heartbeat signals are nonstationary with time-varying rates [1]. In order to estimate the variations of vital sign rates, the landmark-based methods have been proposed to extract the beat-to-beat intervals [23], [24], and convert them into a frequency series. However, the radar-detected heartbeat waveform does not present the sharp peaks as the ECG signal does. Also, the signal distortion, dc offset, and noise may deteriorate the waveform, which makes the landmarks hard to be accurately determined.

Therefore, it is considered that the time–frequency (TF) analysis is effective to provide the local frequency variations along time. The short-time Fourier transform (STFT) has been used for radar heartbeat monitoring [25], but its resolution is strictly limited by the selected window function. The bootstrap-based generalized warblet transform was applied. But it needs an iteration procedure, which is time consuming [26]. Fortunately, the synchrosqueezing transform (SST) is a high-resolution TF algorithm [27], [28]. It is suitable for processing nonstationary signals and has already been used in analyzing some nonstationary signals such as the ECG signal [29] and the seismic data [30]. This algorithm reallocates the coefficients from the wavelet transform to provide a concentrated TF distribution. Moreover, unlike the reassignment technique, it enables separation and reconstruction for the desired signal [31].

In this paper, the noncontact physiological dynamics detection using digital-IF Doppler radar is presented. The digital-IF radar, built from a customized RF module and a field-programmable gate array (FPGA)-based IF module, takes advantages of high sensitivity and low power. By the SST-based signal processing algorithm, high-resolution instantaneous vital sign rates and the corresponding time-domain signals can be extracted. The experimental results show that the SST-based algorithm outperforms the landmark-based method and traditional TF analysis methods. The rest of this paper is organized as follows. The basic theory of the digital-IF radar for noncontact vital sign detection is introduced in Section II. Section III describes the self-designed digital-IF Doppler radar system, and Section IV elaborates the SST-based signal processing algorithm. Then several experiments are carried out in Section V. Finally, the conclusion is given in Section VI.

II. Principle of the Noncontact Instantaneous Vital Sign Detection

The radar considered thereafter transmits a single-tone CW signal, which can be represented as

$$T(t) = \cos[2\pi f t + \phi(t)] \tag{1}$$

where f is the carrier frequency and $\phi(t)$ is the phase noise.

Assuming the distance between the chest wall of a human subject and the radar is $d(t)$, the normalized received signal captured by the radar is

$$\begin{aligned} R(t) &= T\left(t - \frac{2d(t)}{c}\right) \\ &= \cos\left[2\pi f\left(t - \frac{2d(t)}{c}\right) + \phi\left(t - \frac{2d(t)}{c}\right)\right] \end{aligned} \tag{2}$$

where c is the signal propagation speed. According to [10], the distance $d(t)$ consists of a nominal detection distance d_0 and the time-varying chest wall displacement $x(t)$. It should be noted that the amplitude modulation to the received signal is ignored because the chest wall movement $x(t)$ is much smaller than the nominal distance of d_0. Substituting $d(t)$ with $d_0 + x(t)$, the normalized received signal can be written as

$$\begin{aligned} R(t) = \cos\Bigg[&2\pi f t - \frac{4\pi d_0}{\lambda} - \frac{4\pi x(t)}{\lambda} \\ &+ \phi\left(t - \frac{2d_0}{c}\right)\Bigg] \end{aligned} \tag{3}$$

where $\lambda = c/f$ is the wavelength. Because $x(t) \ll d_0$, the change of the phase noise $\phi(t)$ is negligible, and the normalized received signal can be finally approximated as

$$R(t) \approx \cos\left[2\pi f t - \frac{4\pi d_0}{\lambda} - \frac{4\pi x(t)}{\lambda} + \phi\left(t - \frac{2d_0}{c}\right)\right]. \tag{4}$$

It is known that the chest wall displacement $x(t)$ consists of two periodic movements $x_h(t)$ and $x_r(t)$, which are induced by heartbeat and respiration, respectively. Thus, the chest wall displacement can be written as

$$\begin{aligned} x(t) &= x_h(t) + x_r(t) \\ &\approx m_h \sin[2\pi f_h(t)t] + m_r \sin[2\pi f_r(t)t] \end{aligned} \tag{5}$$

where m_h and m_r are the amplitudes of heartbeat and respiration, respectively. $f_r(t)$ and $f_h(t)$ are the time-varying BR and HR, respectively. For a healthy human with normal breath, $f_h(t)$ usually takes value from 0.8 to 1.6 Hz, while $f_r(t)$ ranges from 0.2 to 0.4 Hz.

In the digital-IF radar, the RF signal is first downconverted to IF, which is [19]

$$R_{\mathrm{IF}}(t) \approx \cos\left[2\pi f_{\mathrm{IF}} t + \theta + \frac{4\pi x(t)}{\lambda} + \Delta\phi\right] \tag{6}$$

where f_{IF} is the IF frequency, $\Delta\phi(t) = \phi(t) - \phi(t - 2d_0/c)$ is the residual phase noise, and $\theta = 4\pi d_0/\lambda + \theta_0$ is the constant phase shift dependent on the nominal distance to the target d_0.

Then the analog IF signal is sampled to the digital IF signal directly. Since the null/optimum point problem occurs in a single channel, the quadrature receiver has been adopted to mitigate this problem [10]. Therefore, the digitalized IF signal is downconverted to the digital quadrature baseband signals, which can be represented as [11]

$$B_I(n) = \cos\left[\theta + \frac{4\pi x(n)}{\lambda} + \Delta\phi(n)\right] \tag{7}$$

$$B_Q(n) = \sin\left[\theta + \frac{4\pi x(n)}{\lambda} + \Delta\phi(n)\right] \tag{8}$$

where $n = 1, 2, 3, \ldots, N$ is the sampling points.

As shown in (7) and (8), the instantaneous cardiopulmonary information is involved in the phase information.

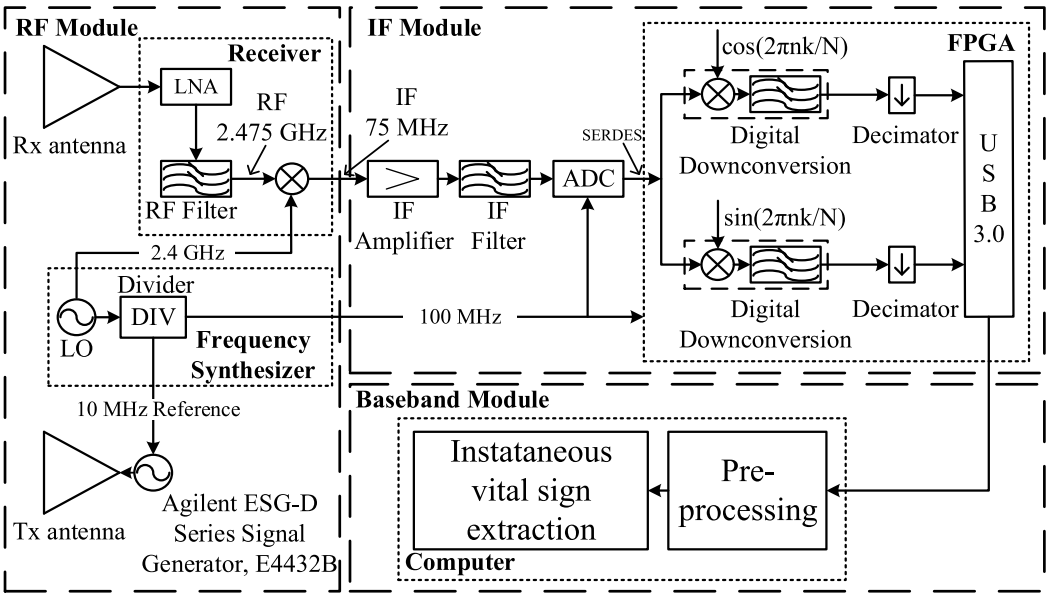

Fig. 1. Block diagram of the heterodyne CW radar including the RF module, IF module, and baseband module.

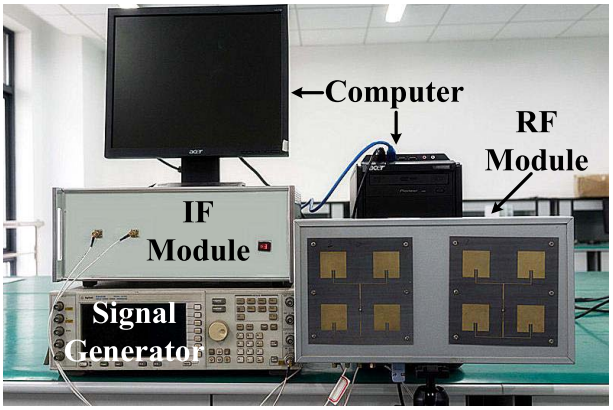

Fig. 2. Photograph of the digital-IF noncontact vital sign detection radar including the RF module, IF module, and baseband module (computer).

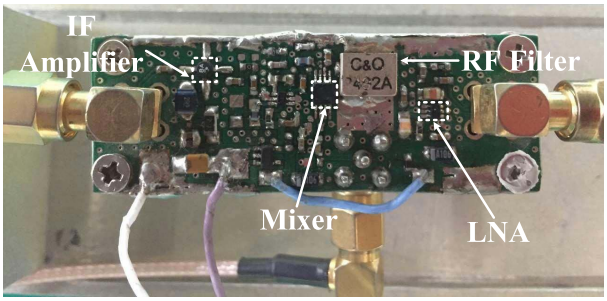

Fig. 3. Photograph of the custom-designed receiver.

Thus, the baseband signal processing is conducted to extract the desired information.

III. Digital-IF CW Doppler Radar

Considering the high accuracy and sensitivity of the digital-IF architecture, we have designed a heterodyne CW Doppler radar with digital-IF receiver to sense tiny vital sign variations. The proposed radar includes an RF module, an IF module, and a baseband module. From the perspective of radar system design and integration, the RF module is custom designed and the IF module is fulfilled in an FPGA. The block diagram and the photograph are shown in Figs. 1 and 2, respectively.

A. RF Module

The RF module can be divided into a transmitting chain and a receiver chain. In the transmitting chain, a pair of 2.4-GHz microchip patch antennas are designed and fixed together for transmitting and receiving. The total size is 161 mm × 161 mm. The gain is 12.8 dB, and the estimated beamwidth is 40°. To make the transmit power adjustable, the Agilent ESG-D series signal generator E4432B is used due to its high stability and low phase noise. The carrier frequency is set at 2.475 GHz.

The receiver is shown in Fig. 3. The received signal is first amplified by an optimized low-noise amplifier, and then filtered by a ceramic filter (RF filter) to realize the image rejection. To ensure the coherence of the entire radar, a high-performance frequency synthesizer is designed with a commercial 2.4-GHz local oscillator (LO) and a commercial frequency divider. It provides three coherent signals, which are the 2.4-GHz LO for the mixer, the 10-MHz RF reference signal for the signal generator, and the 100-MHz reference clock for the FPGA and the analog-to-digital converter (ADC). After mixing, the RF signal is downconverted to the 75-MHz analog IF signal. Then it is sent to the IF module for sampling and digital downconversion.

B. IF Module

In the IF module, a specialized IF filter, whose schematic is shown in Fig. 4, is used to eliminate the out-of-band noise. The 3-dB bandwidth is 71–79 MHz. Thus, the useful 75-MHz IF signal can pass without distortion.

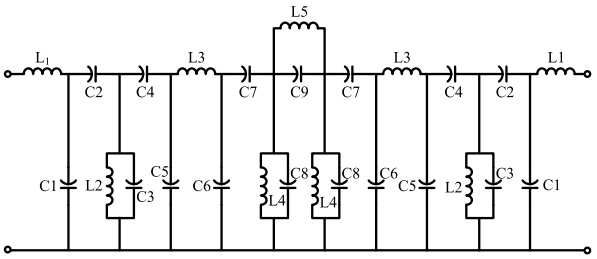

Fig. 4. Schematic of the IF filter.

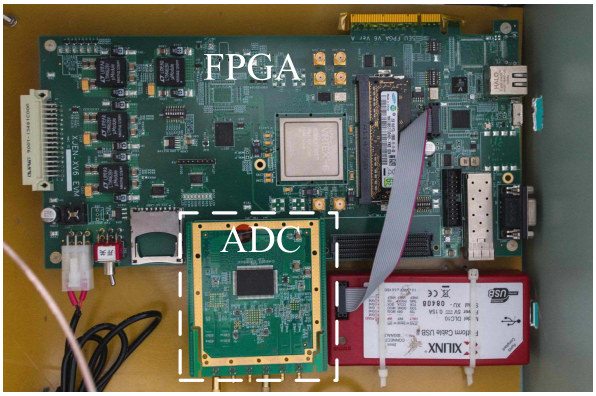

Fig. 5. Photograph of the ADC and Xilinx Virtex-6 FPGA in the IF Module.

The filtered IF signal is digitalized by an ADC with the 100-MHz sampling frequency, which conforms to the band-pass sampling theorem strictly [32]. The digital downconversion is implemented in a Xilinx Virtex-6 (XC6VLX130T) FPGA. Compared with the dedicated components and circuits, the FPGA has great flexibility and stability [33]. The mixing procedures can be realized by the logical operation instead of multiplication. The photograph of the ADC and the FPGA is shown in Fig. 5. The serializer/deserializer protocol is used to connect the ADC and the FPGA, which contributes to mitigate the interference between digital system and analog signal.

In the FPGA, a direct digital synthesizer is used to generate the sine and cosine functions. Then two multipliers, which serve as the downconverters, mix the IF signal with the two functions in the I/Q channels separately. The decimation filter is utilized in each channel to low-pass filter and downsample the I/Q signal to the baseband. Finally, they are transferred to the computer in real time through the universal serial bus 3.0 communication link for subsequent baseband signal processing.

C. Baseband Module

In the proposed radar, the baseband signal processing is implemented in MATLAB. First, the signal quality is improved by some preprocessing, and then the SST-based algorithm is utilized to calculate the instantaneous BR and HR and reconstruct the time-domain signals. The algorithms in detail are elaborated in the next section.

IV. Instantaneous Vital Sign Detection Algorithm

The flowchart of the baseband signal processing algorithm is shown in Fig. 6. As mentioned before, the signal processing

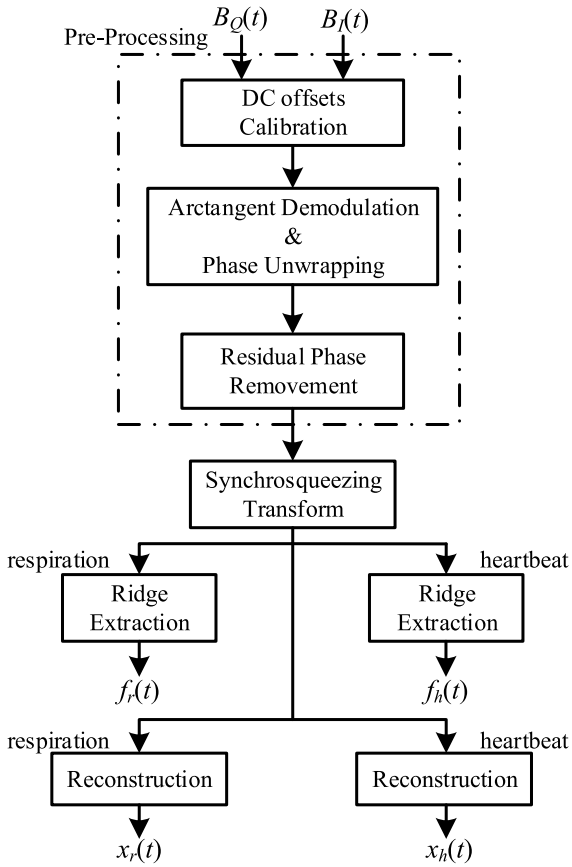

Fig. 6. Baseband signal processing procedure including preprocessing and SST.

algorithm includes signal preprocessing and instantaneous vital sign extraction algorithm. The preprocessing algorithm consists of dc offset calibration, arctangent demodulation, and residual phase removement.

A. Signal Preprocessing

For a quadrature receiver, the I/Q imbalance and the dc offset are two nonignorable problems that deteriorate the demodulation result [11]. However, the digital-IF architecture can eliminate the amplitude imbalance and mitigate the dc offset occurring in the analog homodyne architecture [17]. But, in practice, the dc offset still exists in the baseband signals, which may lead to serious demodulated distortion and decrease the output SNR.

Considering the dc offsets $\mathrm{dc}_I/\mathrm{dc}_Q$, the nonideal baseband I/Q signals become

$$B_I(n) = \cos\left[\theta + \frac{4\pi x(n)}{\lambda} + \Delta\phi(n)\right] + \mathrm{dc}_I \tag{9}$$

$$B_Q(n) = \sin\left[\theta + \frac{4\pi x(n)}{\lambda} + \Delta\phi(n)\right] + \mathrm{dc}_Q. \tag{10}$$

To enhance the demodulation accuracy, the l_p $(0 < p < 1)$ minimization is used to calibrate the dc offsets [34]. Since most measurements can be regarded as sparse, we built a residual sequence $\mathbf{d} = [d_1, d_2, \ldots, d_N]^T$ between an estimated

tuple (a, b, r) and the baseband quadrature measurements $[B_I(n), B_Q(n)]$ as

$$d_n = [B_I(n) - a]^2 + [B_Q(n) - b]^2 - r^2 \tag{11}$$

$$a, b, r \in \mathbb{R} \tag{12}$$

where a and b denote the dc offset in the I and Q channels, respectively. Then we can optimize the sequence $\mathbf{d}$ via the ℓ_p minimization as

$$\min \|\mathbf{d}\|_p^p = \min \|\mathbf{A}\mathbf{x} - \mathbf{y}\|_p^p \tag{13}$$

where

$$\mathbf{A} = \begin{bmatrix} 2B_I(1) & 2B_Q(1) & 1 \\ \cdot & \cdot & \cdot \\ \cdot & \cdot & \cdot \\ \cdot & \cdot & \cdot \\ 2B_I(N) & 2B_Q(N) & 1 \end{bmatrix}, \quad \mathbf{x} = \begin{bmatrix} a \\ b \\ r^2 - a^2 - b^2 \end{bmatrix},$$

$$\mathbf{y} = \begin{bmatrix} B_I(1)^2 + B_Q(1)^2 \\ \cdot \\ \cdot \\ \cdot \\ B_I(N)^2 + B_Q(N)^2 \end{bmatrix}. \tag{14}$$

The nonconvex optimization problem can be solved to obtain $\mathbf{x}$ through the iterative reweighted ℓ_1 algorithm [35]. As a result, the dc offsets can be recovered from the vector $\mathbf{x}$.

The second step is the demodulation and phase unwrapping. The quadrature signals $B_Q(n)$ and $B_I(n)$ are combined by the arctangent operation and phase unwrapping as

$$\begin{aligned} \psi(n) &= \arctan\left[\frac{B_Q(n) - b}{B_I(n) - a}\right] + F \\ &= \theta + \frac{4\pi x(n)}{\lambda} + \Delta\phi(n) \end{aligned} \tag{15}$$

where F is a multiple of 180°.

Since θ and $\Delta\phi(n)$ are nearly constant and useless for the instantaneous frequency extraction, in the third step, they are removed by subtracting the average value as

$$\psi_0(n) = \psi(n) - \frac{1}{N}\sum_{n=0}^{N-1} \psi(n). \tag{16}$$

As shown in (5), a linear combination of $x_h(t)$ and $x_r(t)$ exists, which can be separated by SST on the TF plane if the frequency support of mother wavelet is proper [31]. Meanwhile, SST can present a concentrated distribution while the noise gets spread out across the TF plane [29], so the instantaneous frequencies $f_h(t)$ and $f_r(t)$ can be extracted. Moreover, the time-domain vital sign signals can be reconstructed for further analysis such as heart rate variability and respiratory sinus arrhythmia [24].

B. SST-Based Instantaneous Vital Sign Extraction

In this section, the SST-based algorithm is introduced to extract the instantaneous BR and HR and reconstruct their time-domain signals. The SST is a high-resolution TF algorithm. Since the energy of CWT is spread out over a region around the line of the instantaneous frequency on the time-scale plane, it will be unavoidably smeared by the wavelet function. The SST can reassign the energy distribution of CWT and yield a high-resolution TF representation. In particular, it allows reconstruction for the signals in selected TF region.

According to [27] and [31], the SST algorithm can decompose the signal $f(t)$ into a series of amplitude demodulated–frequency demodulated (AM–FM) signals as

$$s(t) = \sum_{k=1}^{K} s_k(t) \tag{17}$$

where $s_k(t) = A_k(t)\cos[\varphi_k(t)]$ is the AM–FM signal with instantaneous amplitude $A_k(t)$ and frequency $\varphi_k'(t)$ satisfying $\varphi_{k+1}'(t) > \varphi_k'(t)$ for all t.

The algorithm in detail is described as follows [27].

1) Calculate the CWT $W_f(a, b)$ of the signal $f(t)$, which is defined by

$$W_f(a, b) = \int f(t) a^{-1/2} \overline{\nu\left(\frac{t-b}{a}\right)} dt \tag{18}$$

where $\nu(t)$ is the mother wavelet and $\overline{\nu(t)}$ denotes the complex conjugate.

2) For any $W_f(a, b) \neq 0$ on the time-scale plane, calculate the candidate instantaneous frequency as

$$\omega_f(a, b) = -i[W_f(a, b)]^{-1} \frac{\partial W_f(a, b)}{\partial b}. \tag{19}$$

3) Due to the noise in the signal, define a hard threshold parameter $\gamma > 0$ and disregard any points where $|W_f(a, b)| < \gamma$. The SST is defined as [29]

$$T_f(\omega, b) = \int_{A(b)} W_f(a, b) a^{-3/2} \delta(\omega_f(a, b) - \omega) d\omega \tag{20}$$

where $A =: \{a; W_f(a, b) \geq \gamma\}$.

4) According to the frequency ranges of $f_r(t)$ and $f_h(t)$, plot the TF distributions and obtain the instantaneous respiratory frequency $\text{if}_r(t)$ and heartbeat frequency $\text{if}_h(t)$ by extracting their peak energies in the corresponding ranges, which can be represented as

$$\text{if}_r(t) = \underset{w \in [0\ 0.7]\text{Hz}}{\arg\max}\ |T_f(\omega, b)|^2 \tag{21}$$

$$\text{if}_h(t) = \underset{w \in [0.7\ 3]\text{Hz}}{\arg\max}\ |T_f(\omega, b)|^2. \tag{22}$$

To eliminate the possible random fluctuation induced by noise and computational errors, the extracted curves are smoothed by a simple moving average.

5) Let l_r and l_h be the indices of a small frequency band around $\text{if}_r(t)$ and $\text{if}_h(t)$, respectively, the instantaneous time-domain respiratory and heartbeat signals can be reconstructed as

$$x_r(b) = 2\mathcal{R}_v^{-1}\mathfrak{Re}[\int_{l_r} T_f(\omega, b) d\omega] \tag{23}$$

$$x_h(b) = 2\mathcal{R}_v^{-1}\mathfrak{Re}[\int_{l_h} T_f(\omega, b) d\omega] \tag{24}$$

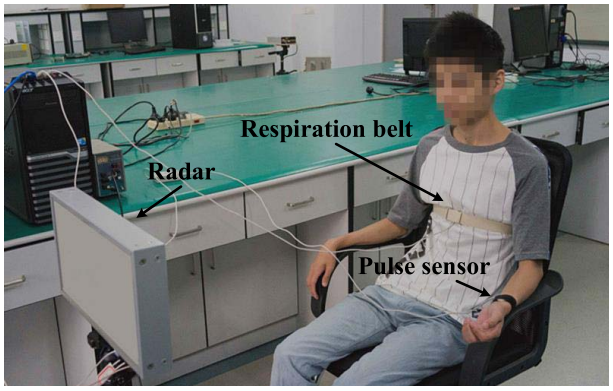

Fig. 7. Photograph of the experimental setup of human vital sign detection.

where

$$\mathcal{R}_v = \int_0^\infty \overline{\hat{v}(\xi)} \frac{d\xi}{\xi} \tag{25}$$

where $\hat{v}(\xi)$ is the Fourier transform of $v(t)$. $\mathcal{R}_v^{-1}$ denotes the reciprocal of $\mathcal{R}_v$.

According to [36], two signals can be separated by SST if the mother wavelet satisfies $\xi_0 \leq (1-\Delta/(1+\Delta))$ where the support in the frequency domain is $[1-\Delta, 1+\Delta]$ and ξ_0 is the ratio of the two frequencies. We know the frequency ratio of heartbeat and respiration is

$$\xi_0 = \frac{f_r(t)}{f_h(t)} \approx 0.3. \tag{26}$$

Then we have $\Delta < (7/(13))$ and the support of $v(t)$ should be smaller than $((6/(13)), (20/(13)))$, so the Morlet wavelet is chosen in the experiments due to the proper frequency support.

V. Experimental Results

To evaluate the proposed algorithm, all experiments have been carried out in a typical indoor laboratory environment. As shown in Fig. 7, the radar was placed so that its signal beam points toward the subject's chest wall. A piezoelectric belt (HKH-11C) and a pulse sensor (HK-2000C) were used to measure the vital sign signals as reference simultaneously.

To extract the time-varying vital sign rates from the reference, the landmark-based method is utilized. First, each peak is manually searched in the time-domain vital sign signal. Then the discrete peak values are sorted into a time series t_i $(i = 1, 2, \ldots)$ with $t_{i+1} > t_i$. As a result, the vital sign rate between successive peaks can be given as

$$R_i = \frac{1}{\Delta t} = \frac{1}{t_{i+1} - t_i}. \tag{27}$$

Finally, the time-varying vital sign rate is smoothed by a moving average filter. The successful detection rate (SDR), which was used in [19], has been used to evaluate the detection accuracy. This parameter is the ratio when the bias between radar-detected and referenced results is less than the given limit in the discrete rate series. The limits we use are 1 beats/min (BPM) for respiration and 3 BPM for heartbeat [19]. The transmit power we use is −13 dBm.

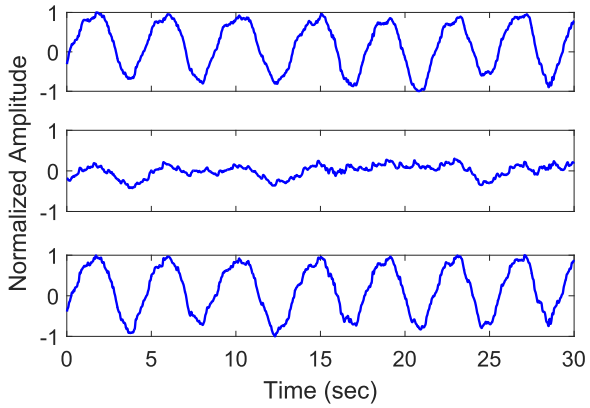

Fig. 8. Quadrature measurements and the preprocessed phase information. The upper trace represents the in-phase measurement. The middle trace represents the quadrature-phase measurement. The lower trace represents the phase information after preprocessing.

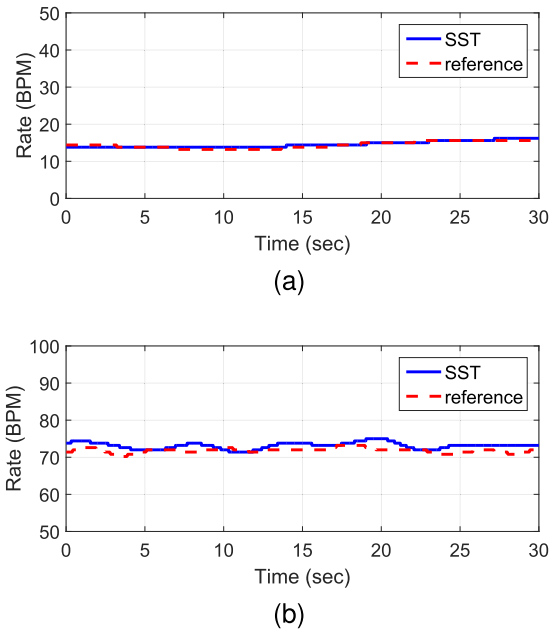

Fig. 9. Instantaneous BR and HR from radar system and reference signals at a 1-m distance. (a) Instantaneous respiratory rate. (b) Instantaneous HR.

TABLE I
SDR of SST-Based and Landmark-Based Methods From Three Distances

Distance (m)	Respiration		Heartbeat	
	SST	landmark	SST	landmark
1	99%	100%	97%	73%
2	100%	86%	97%	49%
3	100%	83%	95%	61%

A. Instantaneous Vital Sign Measurements From Different Distances

The first experiment was carried out at three distances (1, 2, and 3 m) on a healthy male human subject (180 cm, 76 kg). During the experiments, the human subject was asked to sit on a chair and recline against the

TABLE II
SDR OF RADAR-DETECTED INSTANTANEOUS VITAL SIGN RATES FROM FOUR SUBJECTS IN THREE DIFFERENT DISTANCES

Subject	Gender	Height (cm)	Weight (kg)	Respiration			Heartbeat		
				1 m	2 m	3 m	1 m	2 m	3 m
I	Male	172	64.5	100%	100%	100%	97%	96.7%	90.3%
II	Male	171	56	100%	100%	100%	94.8%	90.7%	92%
III	Male	170	70	100%	100%	100%	96.9%	90.2%	93%
IV	Female	155	50.5	100%	100%	100%	95%	93%	91%

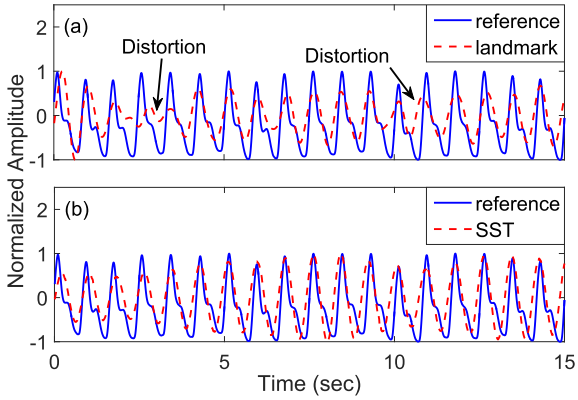

Fig. 10. Time-domain heartbeat signals from the radar and pulse sensor. (a) Result of the landmark-based method. (b) Result of the SST-based method.

chair back while breathing normally. The acquisition time is 30 s. Fig. 8 shows the quadrature measurements detected at 1 m, along with the phase information. Due to the dominant amplitude of respiratory component, it is obvious that the demodulated phase information is periodic and its frequency is around 0.25 Hz (15 BPM).

Fig. 9(a) and (b) presents the instantaneous trajectories of BR and HR derived from the data in Fig. 8, respectively. It is known that the instantaneous BR and HR locate around 15 and 72 BPM, respectively. Compared with the reference, the traces calculated from the proposed method show the high consistency and reliability. Moreover, the tiny fluctuations in the instantaneous HR demonstrate the high resolution of the proposed method.

For comparison, the landmark-based method is also utilized for the radar-detected signal. The SDRs calculated by the landmark-based and proposed methods in each distance are shown in Table I. As widely used in extracting the time-varying frequency, the peak values were determined as the landmarks and used for calculating in Table I [24]. A high-pass filter was applied to separate the heartbeat and respiratory signals. In Table I, it is shown that the proposed algorithm is more accurate and reliable than the landmark-based method. When the detection distance is more than 2 m, the SDR of landmark-based method decreases remarkably, while the proposed method is still accurate. The reason is the proposed algorithm utilizes the complete oscillation period for frequency calculation, which is immune from local peak distortion in the signal.

Fig. 10(a) illustrates the 15-s filtered heartbeat signal waveform from the 1-m measurement. The signal peaks have some obvious distortions or bias, but its oscillator periods still correlate well with the reference. For comparison, the reconstructed heartbeat waveform by the proposed algorithm is plotted in Fig. 10(b). Since the reconstruction is based on the AM–FM model [28], the reconstructed waveform also cannot provide sharp peaks. However, due to the TF selectivity in reconstruction, the reconstructed waveform is more similar to the pure sinusoid than the filtered signal, which equivalents to less distortion. Moreover, its peaks locate close to those in reference waveform, which can be useful for some time-domain analysis.

B. Instantaneous Vital Sign Measurements With Different Human Subjects

To further evaluate the algorithm, some experiments have been carried out on four more human subjects (three males and one female). Similar to the first experiment, the human subjects were also asked to sit on a chair while reclining against the chair back. Each subject was tested with normal breath at three distances (1, 2, and 3 m) in a 30-s period. The SDRs of the four subjects calculated by the proposed algorithm are listed in Table II, along with their characteristics. From Table II, we can see that the instantaneous BR is accurate for all subjects at any distances. Meanwhile, the SDRs of heartbeat are higher than 90% for all the subjects. It is known that when the detection distance increases, the received SNR decreases, and thus the SDR reduces as well.

The reason why the heartbeat detection is more inaccurate than respiratory signal is that the amplitude of chest wall movement induced by heartbeat is weaker than that induced by breath, which can be even less than 1 mm. Moreover, the physiological dynamics are very different among different people. Thus, even at a short detection distance, the received signals may be deteriorated so that the instantaneous rates are inaccurate for some subjects. But the results in Table II demonstrate that the proposed algorithm can provide the reliable estimation of the instantaneous BR and HR with 3 m.

C. Postexercise Instantaneous Vital Sign Measurements

The last experiment was carried out to obtain the postexercise instantaneous vital sign rate during a long time interval. Before the measurement, the volunteer was asked to do some physical exercise for about 5 min to increase his vital sign rate. When he stopped exercising, the volunteer was asked to sit on a chair while reclining against the chair back immediately to recover. Then 120-s data were recorded during his recovery.

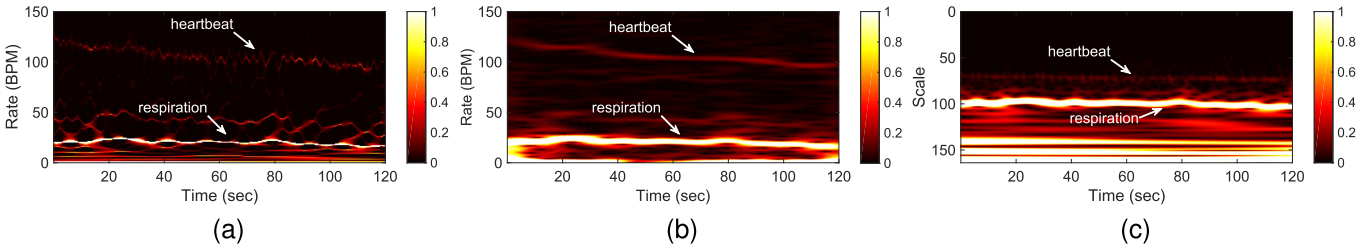

Fig. 11. TF distribution extracted from (a) SST-based algorithm, (b) STFT-based algorithm, and (c) wavelet transform-based algorithm.

In this experiment, the TF distributions by the STFT, the wavelet transform, and SST have been calculated. In Fig. 11, we can see two trajectories in three figures, which correspond to the instantaneous respiratory and heartbeat components. Note that the result from wavelet transform is a time-scale distribution, the y-axis is inversely proportional to the frequency [28]. The instantaneous HR shows a decreasing monoexponential fashion from 120 to 97 BPM [37]. However, the instantaneous BR decreases from 21 to 16 BPM. Comparing the three pictures, the SST can yield the most concentrated TF representation. Some tiny fluctuations in the heartbeat component can be observed only in the SST result. The instability of the instantaneous HR during recovery may be induced by the cardiovascular parasympathetic system [37], [38]. Also, we can identify the second harmonics of the respiratory signal in Fig. 11(b) clearly, which can assist an accurate recovery of the time-domain respiratory signal because typical respiratory movement contains strong second-order harmonic. From this experiment, it is known that the high-resolution instantaneous vital sign rates can be acquired by the proposed algorithm. Furthermore, the radar has the capability of significantly variational instantaneous vital sign rate measurement and long-term monitoring.

VI. Conclusion

In this paper, the noncontact physiological dynamics detection is presented. The SST-based signal processing method was proposed to extract high-resolution instantaneous vital sign rates, as well as to recover their time-domain signals. A custom-designed low-power digital-IF Doppler radar with self-designed RF and FPGA-based IF modules has been presented. Several experiments have been carried out with different volunteers, different distances, and different physiological conditions. The experimental results demonstrate that when radiating a -13 dBm transmit power, our radar can acquire the instantaneous vital signs within 3 m with an SDR of higher than 90%. Therefore, the proposed radar is especially suitable for clinical diagnosis and long-term monitoring.

References

[1] H.-T. Wu, S.-S. Hseu, M.-Y. Bien, Y. R. Kou, and I. Daubechies, "Evaluating physiological dynamics via synchrosqueezing: Prediction of ventilator weaning," *IEEE Trans. Biomed. Eng.*, vol. 61, no. 3, pp. 736–744, Mar. 2014.

[2] G. Benchetrit, "Breathing pattern in humans: Diversity and individuality," *Respirat. Physiol.*, vol. 122, nos. 2–3, pp. 123–129, Sep. 2000.

[3] S. Ahmad, A. Tejuja, K. D. Newman, R. Zarychanski, and A. J. E. Seely, "Clinical review: A review and analysis of heart rate variability and the diagnosis and prognosis of infection," *Crit. Care*, vol. 13, no. 6, pp. 1–7, Dec. 2009.

[4] C. R. Merritt, H. T. Nagle, and E. Grant, "Textile-based capacitive sensors for respiration monitoring," *IEEE Sensors J.*, vol. 9, no. 1, pp. 71–78, Jan. 2009.

[5] P. de Chazal, M. O'Dwyer, and R. B. Reilly, "Automatic classification of heartbeats using ECG morphology and heartbeat interval features," *IEEE Trans. Biomed. Eng.*, vol. 51, no. 7, pp. 1196–1206, Jul. 2004.

[6] C. Li, J. Cummings, J. Lam, E. Graves, and W. Wu, "Radar remote monitoring of vital signs," *IEEE Microw. Mag.*, vol. 10, no. 1, pp. 47–56, Feb. 2009.

[7] Ø. Aardal, Y. Paichard, S. Brovoll, T. Berger, T. S. Lande, and S.-E. Hamran, "Physical working principles of medical radar," *IEEE Trans. Biomed. Eng.*, vol. 60, no. 4, pp. 1142–1149, Apr. 2013.

[8] B. Schleicher, I. Nasr, A. Trasser, and H. Schumacher, "IR-UWB radar demonstrator for ultra-fine movement detection and vital-sign monitoring," *IEEE Trans. Microw. Theory Techn.*, vol. 61, no. 5, pp. 2076–2085, May 2013.

[9] Y. Nijsure *et al.*, "An impulse radio ultrawideband system for contactless noninvasive respiratory monitoring," *IEEE Trans. Biomed. Eng.*, vol. 60, no. 6, pp. 1509–1517, Jun. 2013.

[10] A. D. Droitcour, O. Boric-Lubecke, V. M. Lubecke, J. Lin, and G. T. A. Kovacs, "Range correlation and I/Q performance benefits in single-chip silicon Doppler radars for noncontact cardiopulmonary monitoring," *IEEE Trans. Microw. Theory Techn.*, vol. 52, no. 3, pp. 838–848, Mar. 2004.

[11] C. Li, Y. Xiao, and J. Lin, "Experiment and spectral analysis of a low-power Ka-band heartbeat detector measuring from four sides of a human body," *IEEE Trans. Microw. Theory Techn.*, vol. 54, no. 12, pp. 4464–4471, Dec. 2006.

[12] Y. Yang, C. Gu, Y. Li, R. Gale, and C. Li, "Doppler radar motion sensor with CMOS digital DC-tuning VGA and inverter-based sigma-delta modulator," *IEEE Trans. Instrum. Meas.*, vol. 63, no. 11, pp. 2666–2674, Nov. 2014.

[13] M. Zakrzewski *et al.*, "Quadrature imbalance compensation with ellipse-fitting methods for microwave radar physiological sensing," *IEEE Trans. Microw. Theory Techn.*, vol. 62, no. 6, pp. 1400–1408, Jun. 2014.

[14] S. Bakhtiari *et al.*, "Compact millimeter-wave sensor for remote monitoring of vital signs," *IEEE Trans. Instrum. Meas.*, vol. 61, no. 3, pp. 830–841, Mar. 2012.

[15] S. Guan, J. A. Rice, C. Li, and C. Gu, "Automated DC offset calibration strategy for structural health monitoring based on portable CW radar sensor," *IEEE Trans. Instrum. Meas.*, vol. 63, no. 12, pp. 3111–3118, Dec. 2014.

[16] C. Gu *et al.*, "Accurate respiration measurement using DC-coupled continuous-wave radar sensor for motion-adaptive cancer radiotherapy," *IEEE Trans. Biomed. Eng.*, vol. 59, no. 11, pp. 3117–3123, Nov. 2012.

[17] C. Li, V. M. Lubecke, O. Boric-Lubecke, and J. Lin, "A review on recent advances in doppler radar sensors for noncontact healthcare monitoring," *IEEE Trans. Microw. Theory Techn.*, vol. 61, no. 5, pp. 2046–2060, May 2013.

[18] Y. Wu and J. Li, "The design of digital radar receivers," *IEEE Aerosp. Electron. Syst. Mag.*, vol. 13, no. 1, pp. 35–41, Jan. 1998.

[19] C. Gu, C. Li, J. Lin, J. Long, J. Huangfu, and L. Ran, "Instrument-based noncontact Doppler radar vital sign detection system using heterodyne digital quadrature demodulation architecture," *IEEE Trans. Instrum. Meas.*, vol. 59, no. 6, pp. 1580–1588, Jun. 2010.

[20] C. Li, J. Ling, J. Li, and J. Lin, "Accurate Doppler radar noncontact vital sign detection using the RELAX algorithm," *IEEE Trans. Instrum. Meas.*, vol. 59, no. 3, pp. 687–695, Mar. 2010.

[21] L. Sun, Y. Li, H. Hong, F. Xi, W. Cai, and X. Zhu, "Super-resolution spectral estimation in short-time non-contact vital sign measurement," *Rev. Sci. Instrum.*, vol. 86, no. 4, p. 044708, 2015.

[22] L. Sun *et al.*, "Noncontact vital sign detection based on stepwise atomic norm minimization," *IEEE Signal Process. Lett.*, vol. 22, no. 12, pp. 2479–2483, Dec. 2015.

[23] W. Hu, Z. Zhao, Y. Wang, H. Zhang, and F. Lin, "Noncontact accurate measurement of cardiopulmonary activity using a compact quadrature Doppler radar sensor," *IEEE Trans. Biomed. Eng.*, vol. 61, no. 3, pp. 725–735, Mar. 2014.

[24] W. Massagram, V. M. Lubecke, A. Høst-Madsen, and O. Boric-Lubecke, "Assessment of heart rate variability and respiratory sinus arrhythmia via doppler radar," *IEEE Trans. Microw. Theory Techn.*, vol. 57, no. 10, pp. 2542–2549, Oct. 2009.

[25] W. Hu, H. Zhang, Z. Zhao, Y. Wang, and X. Wang, "Real-time remote vital sign detection using a portable Doppler sensor system," in *Proc. IEEE Sensors Appl. Symp. (SAS)*, Feb. 2014, pp. 89–93.

[26] S. Kazemi, A. Ghorbani, H. Amindavar, and D. R. Morgan, "Vital-sign extraction using bootstrap-based generalized warblet transform in heart and respiration monitoring radar system," *IEEE Trans. Instrum. Meas.*, vol. 65, no. 2, pp. 255–263, Feb. 2016.

[27] I. Daubechies, J. Lu, and H.-T. Wu, "Synchrosqueezed wavelet transforms: An empirical mode decomposition-like tool," *Appl. Comput. Harmon. Anal.*, vol. 30, no. 2, pp. 243–261, Mar. 2011.

[28] G. Thakur, E. Brevdo, N. S. Fučkar, and H.-T. Wu, "The synchrosqueezing algorithm for time-varying spectral analysis: Robustness properties and new paleoclimate applications," *Signal Process.*, vol. 93, no. 5, pp. 1079–1094, May 2013.

[29] H.-T. Wu, Y.-H. Chan, Y.-T. Lin, and Y.-H. Yeh, "Using synchrosqueezing transform to discover breathing dynamics from ECG signals," *Appl. Comput. Harmon. Anal.*, vol. 36, no. 2, pp. 354–359, Mar. 2014.

[30] P. Wang, J. Gao, and Z. Wang, "Time-frequency analysis of seismic data using synchrosqueezing transform," *IEEE Geosci. Remote Sens. Lett.*, vol. 11, no. 12, pp. 2042–2044, Dec. 2014.

[31] F. Auger *et al.*, "Time-frequency reassignment and synchrosqueezing: An overview," *IEEE Signal Process. Mag.*, vol. 30, no. 6, pp. 32–41, Nov. 2013.

[32] R. G. Vaughan, N. L. Scott, and D. R. White, "The theory of bandpass sampling," *IEEE Trans. Signal Process.*, vol. 39, no. 9, pp. 1973–1984, Sep. 1991.

[33] Y. Wang, Q. Liu, and A. E. Fathy, "CW and pulse–Doppler radar processing based on FPGA for human sensing applications," *IEEE Trans. Geosci. Remote Sens.*, vol. 51, no. 5, pp. 3097–3107, May 2013.

[34] H. Zhao, H. Hong, L. Sun, F. Xi, C. Li, and X. Zhu, "Accurate DC offset calibration of Doppler radar via non-convex optimisation," *Electron. Lett.*, vol. 51, no. 16, pp. 1282–1284, Aug. 2015.

[35] R. Chartrand, "Exact reconstruction of sparse signals via nonconvex minimization," *IEEE Signal Process. Lett.*, vol. 14, no. 10, pp. 707–710, Oct. 2007.

[36] H.-T. Wu, P. Flandrin, and I. Daubechies, "One or two frequencies? the synchrosqueezing answers," *Adv. Adapt. Data Anal.*, vol. 3, nos. 1–2, pp. 29–39, Apr. 2011.

[37] M. Buchheit, Y. Papelier, P. B. Laursen, and S. Ahmaidi, "Noninvasive assessment of cardiac parasympathetic function: Postexercise heart rate recovery or heart rate variability?" *Amer. J. Physiol. Heart Circ. Physiol.* vol. 293, pp. 8–10, Mar. 2007.

[38] R. Karasik *et al.*, "Correlation differences in heartbeat fluctuations during rest and exercise," *Phys. Rev. E, Stat. Phys. Plasmas Fluids Relat. Interdiscip. Top.*, vol. 66, no. 6, p. 062902, Dec. 2002.

Heng Zhao (S'14) received the B.S. degree from the Nanjing University of Science and Technology, Nanjing, China, in 2012, where he is currently pursuing the Ph.D. degree.

From 2015 to 2016, he was a Research Assistant with Texas Tech University, Lubbock, TX, USA. His current research interests include radar signal processing, and biomedical application of microwave and RF circuits and systems.

Hong Hong (M'10) received the Ph.D. degree in electrical engineering from Nanjing University, Nanjing, China, in 2010.

Since 2010, he has been a Lecturer with the Nanjing University of Science and Technology, Nanjing. In 2014, he was a Visiting Scholar with the Institute of Biomedical Engineering and Technology, Sydney University, Sydney, NSW, Australia. His current research interests include biomedical radar applications of microwave and RF circuits and systems, speech signal processing, and radar signal processing.

Li Sun (M'16) received the Ph.D. degree from the Nanjing University of Science and Technology, Nanjing, China, in 2016.

His current research interests include radar signal processing, compressed sensing and super-resolution technique, and biomedical application of microwave and RF circuits and systems.

Yusheng Li (M'07) received the M.S. degree from the Nanjing University of Science and Technology, Nanjing, China, in 2004.

Since 2010, he has been a Lecturer with the Nanjing University of Science and Technology, Nanjing. His current research interests include radar system, radar signal processing, and biomedical radar applications of microwave and RF circuits and systems.

Changzhi Li (S'06–M'09–SM'13) received the B.S. degree in electrical engineering from Zhejiang University, Hangzhou, China, in 2004, and the Ph.D. degree in electrical engineering from the University of Florida, Gainesville, FL, USA, in 2009.

From 2007 to 2009, he was first with Alereon Inc., Austin, TX, USA, and then with Coherent Logix Inc. Austin, where he was involved with ultrawideband transceivers and software-defined radio, respectively. He joined Texas Tech University, Lubbock, TX, USA, as an Assistant Professor in 2009, and became an Associate Professor in 2014. His current research interests include biomedical applications of microwave technology, wireless sensors, and RF/analog circuits.

Dr. Li is an Associate Editor of the IEEE TRANSACTIONS ON CIRCUITS AND SYSTEMS I. He served as an Associate Editor of the IEEE TRANSACTIONS ON CIRCUITS AND SYSTEMS II in 2014 and 2015. He served as the TPC Co-Chair of the IEEE Wireless and Microwave Technology Conference in 2012 and 2013. He was a recipient of the IEEE Sensors Council Early Career Technical Achievement Award, the ASEE Frederick Emmons Terman Award, the IEEE-HKN Outstanding Young Professional Award, the NSF Faculty Early CAREER Award, and the IEEE MTT-S Graduate Fellowship Award. He received nine best conference/student paper awards as author/advisor in IEEE-sponsored conferences.

Xiaohua Zhu (M'07) received the Ph.D. degree in communication and information system from the Nanjing University of Science and Technology, Nanjing, China, in 2002.

He is currently a Professor with the School of Electronic and Optical Engineering, Nanjing University of Science and Technology. He has authored or co-authored four books, and more than 100 papers. He has submitted 18 patent applications. His current research interests include radar system, radar signal theory, and digital signal processing.

Dr. Zhu is the Leader of Radar and High-speed Digital Signal Processing Laboratory at the Nanjing University of Science and Technology. He received the Ministerial and Provincial-Level Science and Technology Award ten times.